Factors Causing Stratocumulus to Deviate from Subtropical High Variability on Seasonal to Interannual Timescales

Hairu Ding[1], Bjorn Stevens[1], and Hauke Schmidt[1]

[1]Max Planck Institute for Meteorology, Hamburg, Germany

Correspondence: Hairu Ding (hairu.ding@mpimet.mpg.de)

Abstract. Stratocumulus (Sc) covers the eastern flanks of maritime subtropical high-pressure systems, and changes in their coverage can exert a radiative effect on the global energy budget comparable to that of a doubling of CO_2. Previous studies have identified the temperature difference between $700\,\mathrm{hPa}$ and the surface as the primary driver of Sc variability. However, the mechanistic linkages between subtropical highs and this critical temperature difference, which defines lower tropospheric stability, remain unresolved. While subsidence modulates temperatures at $700\,\mathrm{hPa}$ and wind-driven cooling affects surface temperatures, the observed decoupling between subtropical highs and Sc fraction on seasonal to interannual timescales lacks a mechanical explanation. This study uses reanalysis data to test two hypothesized pathways linking subtropical highs to the lower tropospheric stability. Results demonstrate that neither pathway dominates, as correlations between Sc-area temperatures and subtropical high dynamics exhibit strong regional and temporal dependencies. Additionally, Sc-area conditions do not systematically align with subtropical high variability, highlighting the need for further investigation into the dynamical processes governing temperatures in the lower troposphere.

1 Introduction

Stratocumulus (Sc), which covers around 20% of the low-latitude oceans, plays an important role in the global energy budget by reflecting solar radiation (Warren et al., 1986, 1988; Hahn and Warren, 2007; Wood, 2012). Previous studies have verified that changes in their fraction of only 3–5% can lead to effects commensurate with those from a doubling of atmospheric CO_2 concentrations (Hartmann and Short, 1980; Randall and Suarez, 1984; Slingo, 1990), a fact that has motivated a considerable amount of research, including this study, to understand what controls Sc variations and changes.

To understand the variation of Sc, one approach has been to identify and study cloud controlling factors (Stevens and Brenguier, 2009). Previous researchers have made progressive efforts to define such factors statistically. For instance, already a century ago it was appreciated that Sc are sensitive to the temperature and humidity difference between the surface and air above the clouds (Blake, 1928). It is now understood that the sensitivity to the temperature difference arises because this difference measures the stability of the Sc-top interface, whereby greater stability suppresses the entrainment velocity, which limits the entrainment drying that inhibits cloud formation. Likewise for a given entrainment rate, a drier free atmosphere implies more entrainment drying. Klein and Hartmann (1993) made these relationships quantitative by demonstrating a strong and linear relationship between lower-tropospheric stability (LTS), which they defined as the difference between $700\,\mathrm{hPa}$ and

$1000\,\mathrm{hPa}$, and variations in Sc amount across regions and seasons. Later, Wood and Bretherton (2006) introduced the estimated inversion strength (EIS) to account for differences in lapse rates that influence the relationship between θ at $700\,\mathrm{hPa}$ and its more pertinent value, which lies just above cloud top. They found that EIS explains the variation of low clouds across a wider range of temperature regimes, and hence latitudes, to provide good predictions across tropical, subtropical, and mid-latitude regions. Kawai et al. (2017) combined EIS with the humidity difference into a unified index which they called estimated cloud top entrainment index (ECTEI). They tested ECTEI using ship observations and found it correlates with the total low stratiform clouds (including Sc, stratus, and sky-obscuring fog) better than EIS. Apart from the role of temperature and humidity differences, a physical understanding of Sc identifies a variety of other physical factors, including, large-scale atmospheric subsidence (Weaver and Pearson Jr, 1990; Randall and Suarez, 1984), downwelling longwave radiation above clouds (Stevens and Brenguier, 2009), and sea surface temperature (SST) (Klein et al., 1995).

Based on those factors, and from the spatial coincidence of Sc on the eastern-flanks of the semi-permanent subtropical high-pressure regions, an expectation arises that variations in these high-pressure regions will influence Sc. We identify two hypothesized pathways by which the variation of subtropical highs may affect neighboring regions of Sc. The first hypothesized mechanism would be that variations in the subsidence influence the free-tropospheric temperature above Sc, and hence Sc themselves, through enhanced adiabatic warming. If this hypothesis holds, it suggests that variability in Sc may be linked to remote monsoon regions. The pioneering work of Rodwell and Hoskins (1996) has shown a teleconnection between monsoons and subtropical subsidence described as a “monsoon-desert mechanism". Latent heat release from monsoonal convection generates a westward-propagating Rossby wave that enhances subtropical subsidence, subsequently influencing the free-tropospheric temperature. The second hypothesized mechanism is that variations in the steepness of the high, as measured by the zonal geopotential gradients from its mass center to the east coast, change surface temperatures through their effect on near-surface winds and the winds' consequent effects on surface currents, ocean upwelling, and surface cooling via wind-driven evaporation. Some evidence for such relationships exists, based on studies that have found Sc to co-vary with the subtropical highs on synoptic (Klein et al., 1995; Klein, 1997; George and Wood, 2010; Toniazzo et al., 2011) and diurnal timescales (Ciesielski et al., 2001; Duynkerke and Teixeira, 2001; Garreaud and Muñoz, 2004). However, these relationships are not particularly strong. Moreover, there is scant evidence for such relationships on seasonal and interannual timescales, in which LTS dominants Sc variation (Klein and Hartmann, 1993; Wood and Bretherton, 2006; Richter and Mechoso, 2004, 2006). A few studies that have addressed this question have found the subtropical highs to be less important than the LTS itself (McCoy et al., 2017; Qu et al., 2015; Zhou et al., 2015). The extent to which this holds up to a more systematic analysis, and if so whether it is due to confounding influences, or simply by the fact that the strength of highs is a poor predictor of the constituent terms of cloud controlling factors, as identified through a statistical analysis, is the focus of the present study. To test the first hypothesized mechanism, we analyze whether subsidence, characterized by ω_{700}, warms the free troposphere adiabatically. Similarly, $\frac{\mathrm{d}\Phi}{\mathrm{d}x}$ represents the steepness of the high in the second hypothesized mechanism, whose changes may influence wind stress, ocean upwelling, and surface temperature. Both factors are selected to describe the features of subtropical highs because they are physically connected to mechanisms proposed to influence EIS. Another commonly used factor for subtropical highs—sea

level pressure (SLP)—is tested not to be a good representor for both ω_{700} and $\frac{\mathrm{d}\Phi}{\mathrm{d}x}$ to investigate the mechanical relationship between subtropical highs and EIS.

Specifically we test the two hypothesized pathways by which the subtropical high-pressure systems may influence cloud amount in the main Sc areas. This requires defining the main Sc areas and the high-pressure areas based on the data, as described in §2, and identifying whether the quantities hypothesized to be regulated by variations in the subtropical high are indeed the dominant cloud controlling factors. We first establish a metric for Sc amount (§2.2) and use this to investigate the contributions of the free-tropospheric and the surface pathways to the variation of Sc in §3.1. Then, the free-tropospheric pathway is tested in §3.2 and the surface pathway in §3.3. The investigation of free-tropospheric pathway follows the logic of how subsidence impacts adiabatic processes (Figs. 4, 5) and hence the potential temperature at $700\,\mathrm{hPa}$ (Fig. 6). In addition, the surface pathway is tested through the impact of geopotential gradient on ocean upwelling and latent heat flux (Fig. 7), and thus changes the potential temperature at $1000\,\mathrm{hPa}$ (Fig. 8). Finally, the correlation between variables in the Sc and subtropical high areas is tested in §3.4. The conclusions drawn from our analyses are presented in §4.

2 Data and Methods

2.1 Data

This paper uses ERA5 (the fifth generation ECMWF atmospheric reanalysis, E5, Hersbach et al. 2017) data for cloud controlling factors and atmospheric conditions. Its data is provided on a $0.25^\circ \times 0.25^\circ$ grid, with three-dimensional fields on 37 pressure levels. The monthly mean of SLP, surface latent heat flux, wind components, vertical velocity, temperature, and geopotential heights are analyzed.

Low cloud fraction is analyzed based on the satellite data. This paper uses the second version of the ATSR-AATSR (Along-Track Scanning Radiometer and Advanced Along-Track Scanning Radiometer) data set in the Cloud_cci (European Space Agency Climate Change Initiative) project (Poulsen et al. (2017)). The data are provided on a $0.5^\circ \times 0.5^\circ$ grid. In this paper, Sc amount is denoted by the symbol κ and defined to be equal to the low cloud fraction (cfc_low) in the identified Sc areas (see Section 2.2.2.1). ATSR-AATSR features a two-view radiometer with 7 channels and is one of a number of cloud climatologies that we chose because it is associated with essential climate variables (details are available at https://space.oscar.wmo.int/instruments/view/aatsr).

For the ATSR-AATSR data, monthly means for the period from January 2003 to December 2011 are analyzed and compared to ERA5 data over the same period. For the analyses of mechanisms that impact the cloud controlling factors, the 30-year ERA5 record, from January 1985 to December 2014, is analyzed. To fix terminology, our use of the term “seasonal cycle" denotes the monthly climatology, while the term “interannual" denotes the variations in specific monthly values across the record—July for the Northern Hemisphere and January for the Southern Hemisphere. These months are chosen because subtropical highs are at their peak intensity, and Sc reaches its maximum during the summertime, when the monsoon-desert mechanism intensifies subsidence in their vicinity. We have also examined the interannual variability during the winter season, and the results are consistent with those observed during the summertime period. The “climatological mean" refers to the average over all months

for the thirty-year record. Hence, for the thirty-year ERA data, at each spatial location, the seasonal cycle has 12 data points, the interannual record has 30-point records, and the climatological mean has one data point.

2.2 Definitions

A variety of quantities arise in our analysis and are defined as described as follows. In addition to defining the areas over which the analysis is performed, and the various cloud controlling factors being considered, two additional quantities are defined as possible pathways by which the variation of the subtropical highs might influence cloud-controlling factors and hence cloudiness, κ.

2.2.1 Marine subtropical highs and stratocumulus areas

Marine subtropical highs are defined by the union of closed $1020\,\mathrm{hPa}$ contours of the climatological-mean SLP and marine areas. These are referred to subtropical high areas (H-areas) and denoted by color in Figure 1. Five major regions can be identified across the globe, and these are named, respectively, North Pacific (NP), North Atlantic (NA), South Pacific (SP), South Atlantic (SA), and South Indian Ocean (SI).

Similarly, Sc areas (c-areas) are defined when the mean low cloud fraction of 9 years is greater than 0.5 (or 0.4 for NA) and falls within 45°N–45°S. c-areas are shown as thick black contours in Fig. 1. Figure 1 shows the c-areas are typically located eastward of H-areas.

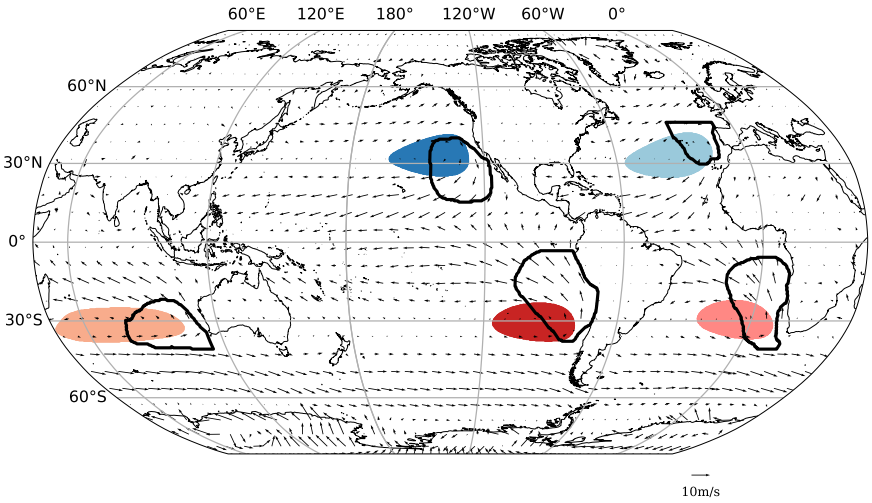

Figure 1. The defined H-areas (shaded) and c-areas (thick black lines). The quivers denote $10\,\mathrm{m}$ wind field. Each color represents one region, and it is consistent in the later analyses. The map uses the Robinson projection.

This paper uses some similar words to address different concepts. “Regions" specifies the difference among NP, NA, SI, SP, and SA. “Areas" specifies the difference between H- and c-areas. Subscripts "H" and "c" represent the area over which the variables are averaged.

2.2.2 Cloud controlling factors

Previous studies suggested four factors to represent lower tropospheric conditions: the hydro-lapse ($\mathscr{H}$), LTS, EIS, ECTEI (Klein and Hartmann, 1993; Wood and Bretherton, 2006; Kawai et al., 2017), as defined below:

$\mathscr{H}$: The hydro-lapse is defined as

$$\mathscr{H} = \beta \frac{l_{\mathrm{v}}}{c_p}(q_{700} - q_{1000}) \tag{1}$$

where β = 0.23, l_{v} is the latent heat of vaporization, c_p is the specific heat of air at constant pressure, and q is the specific humidity. Here, and throughout, a numeric subscript denotes the pressure level in units of hPa

LTS**:** The lower-tropospheric stability is defined as:

$$\mathrm{LTS} = \theta_{700} - \theta_{1000} \tag{2}$$

where θ is the potential temperature.

EIS**:** The estimated inversion strength is defined as:

$$\mathrm{EIS} = \mathrm{LTS} - \Gamma_{850}\,(Z_{700} - \mathrm{LCL}) \tag{3}$$

where Γ denotes the moist lapse rate, and Γ_{850} is calculated by the average temperature of 700 and $1000\,\mathrm{hPa}$. Z denotes the geopotential height. LCL is the lifting condensation level. To estimate the LCL we assume a constant surface relative humidity of 80%, consistent with Wood and Bretherton (2006). Based on the approximations $\mathrm{RH} \approx 100 - 5(T - T_{\mathrm{d}})$ and $\mathrm{LCL} \approx 125(T - T_{\mathrm{d}})$ with RH in %, LCL in m, and T and T_{d} in K, from Lawrence (2005), the difference between surface temperature and dew point is approximately $4\,\mathrm{K}$, and the corresponding LCL is about $500\,\mathrm{m}$.

ECTEI**:** The estimated cloud top entrainment index is defined as:

$$\mathrm{ECTEI} = \mathrm{EIS} + \mathscr{H} \tag{4}$$

Some recent studies re-evaluated LTS and EIS and found that they have little difference in their ability to describe cloud amounts and that this difference varies with data sources (Cutler et al., 2022; Park and Shin, 2019). For this reason we re-examine the correlation between each suggested factor and κ to select the one that is the best predictor. Figure 2 shows that EIS best explains variations in κ across all monthly means. Analyses of the same correlations on both the seasonal ($r = 0.93$) and the interannual ($r = 0.79$) timescales are consistent with the results based on all monthly means. Hence, EIS is selected for the

following investigation. The performance of $\mathscr{H}$ is the worst. Even though $\mathscr{H}$ and κ are correlated at least in SP and SA, also in these regions the correlations weaker than those between κ and the other factors. This agrees with Klein and Hartmann (1993), which claims that moisture dominates the change of stratus in the Arctic but not for subtropical Sc. For this reason (which through a supplementary analysis we also confirm, but don't include here) the effects of subtropical highs on Sc through the influence of their variations on the the free tropospheric humidity are not explored further.

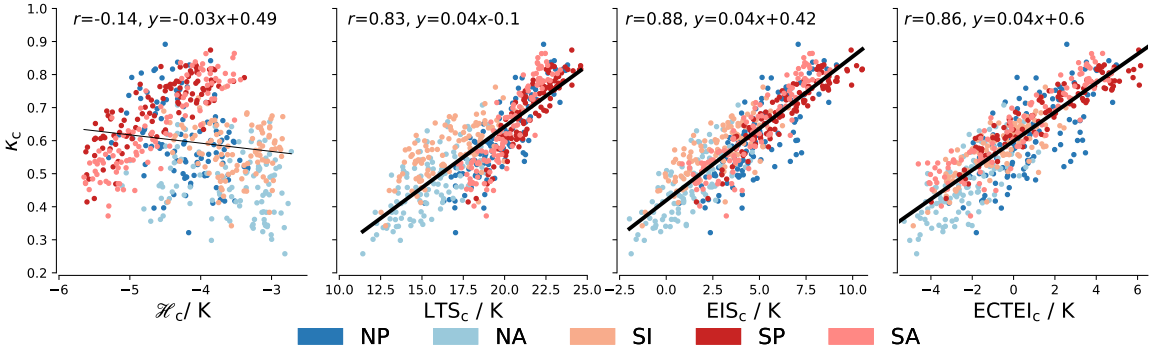

Figure 2. Scatter plots of different cloud controlling factors and low cloud fraction (κ) from 2003 to 2011. Each scatter point represents a monthly mean, and the plots include 9 years of data, covering all 12 months per year. From left to right, the cloud controlling factors are $\mathscr{H}$, LTS, EIS, ECTEI, analyzed over the cloud (c) areas, as denoted by subscript. All subplots share the same y-axis, which represents κ, with each plot displaying data points colored by different regions. Regression lines are presented for p-values ≤ 0.05, and thickened when $r^2 \geq 0.25$.

2.2.3 Adiabatic warming of lower-free troposphere

For a stronger high-pressure we expect greater subsidence and more adiabatic warming, which in the mean would need to be balanced by increased radiative cooling or advection.

To explore the link between the lower-tropospheric potential temperature and the high-pressure regions we look to the thermodynamic energy equation. There, assuming stationarity, adiabatic warming (Q) must be balanced by diabatic warming/-cooling (Q_{Diab}), such that:

$$Q = -Q_{\mathrm{Diab}} = -(\boldsymbol{v} \cdot \nabla\theta + \omega \frac{\partial\theta}{\partial p}) \tag{5}$$

Here $\boldsymbol{v} \cdot \nabla\theta$ denotes horizontal advection, with $\boldsymbol{v}$, the horizontal wind vector, and $\omega \frac{\partial\theta}{\partial p}$ describes vertical advection, with ω representing vertical (pressure) velocity, and p denoting the pressure. Q_{Diab} can be associated with the convergence of radiant energy, or through turbulent mixing associated with covariances arising from the use of mean quantities to form the budget terms.

2.2.4 Wind driven surface cooling

According to our second hypothesis, a high pressure system with a larger zonal geopotential gradient ($\frac{\mathrm{d}\Phi}{\mathrm{d}x}$) would be accompanied by a cooler surface. This could be due to a variety of mechanisms. First, it leads to more equatorward winds due to the geostrophic balance:

$$v = \frac{1}{f}\frac{\mathrm{d}\Phi}{\mathrm{d}x} \tag{6}$$

where Φ is the geopotential, x represents distance in the zonal direction, f is the Coriolis parameter, and we analyze $\frac{\mathrm{d}\Phi}{\mathrm{d}x}$ at $700\,\mathrm{hPa}$.

The consequently increased surface wind-stress leads to more ocean upwelling and hence surface cooling. This upwelling is measured by the Ekman pumping velocity, w_E :

$$w_\mathrm{E} = \nabla \times \left(\frac{\boldsymbol{\tau}}{\rho_0 f}\right). \tag{7}$$

Here $\rho_0 = 1030\,\mathrm{kg\,m^{-3}}$ is the density of ocean water, and

$$\boldsymbol{\tau} = \boldsymbol{v_{10}} \cdot \rho_\mathrm{a} C_\mathrm{D} \|V\| \tag{8}$$

is the surface wind-stress, with $\rho_\mathrm{a} = 1.225\,\mathrm{kg\,m^{-3}}$ the density of near-surface air, C_D the drag coefficient, $\boldsymbol{v_{10}}$ the near-surface ($10\,\mathrm{m}$) horizontal wind, and $\|V\|$ the near-surface wind speed. Since wind speeds are moderate in subtropical high and Sc regions, the drag coefficient C_D is assumed to be constant at 0.0012, following Large and Pond (1981). A positive value of w_E means upwelling motion, and a negative means downwelling motion. Different from other variables, the w_E is analyzed in a continuous area of positive w_E near the coast.

In addition, increased surface winds can also cool the surface through enhanced evaporation, which is measured by the latent heat flux (LHF).

3 Analysis

In this section we first explore what factors explain variations in EIS, which we now use as a proxy for cloudiness κ. We then explain to what extent these factors can be related to variations of the subtropical high-pressure regions.

3.1 Dependence of EIS on θ_{700} and θ_{1000}

EIS differs from LTS as it includes the temperature-dependent lapse rate Γ, but it is dominated by the variations of LTS (i.e., the difference between θ_{700} and θ_{1000}) because any change in lapse rates depends on the change of the temperature below 700 hPa. Table 1 shows how these quantities vary across different regions and for different timescales and how much they contribute to variability in EIS.

In the higher latitude regions of the NP, NA and SI, variations of θ_{700} are mostly larger than variations in θ_{1000} in both the seasonal and interannual data and explain a large part of the variability in EIS in those regions, particularly on seasonal

timescales. In these regions θ_{700} and θ_{1000} strongly co-vary across the seasonal cycle, but θ_{700} varies more. This means that EIS increases even as θ_{1000} increases, which explains the otherwise counterintuitive positive correlation between θ_{1000} and EIS in the higher-latitude regions on seasonal timescales. For the more equatorward regions of the SP and SA, variability of EIS is dominated by θ_{1000}, of which the variability is much larger than that of θ_{700} on seasonal timescales. This result is consistent with Klein and Hartmann (1993), who found that lower tropospheric stability covaries with θ_{700} in NP, NA, and SI, and with SST in other regions. Moreover, variations in θ_{1000} are important for all regions on interannual timescales (as evidenced by the correlations between θ_{1000} and EIS in Table 1), and are particularly important for the main Sc areas of the NP, SA, as well as for the SI, where the standard deviations of θ_{1000} and θ_{700} are nearly equal.

c-area	Seasonal Cycle						Interannual Variability					
	$\theta_{1000,\mathrm{c}}$		$\theta_{700,\mathrm{c}}$		$\omega_{700,\mathrm{H}}$		$\theta_{1000,\mathrm{c}}$		$\theta_{700,\mathrm{c}}$		$\omega_{700,\mathrm{H}}$	
	r	σ/K	r	σ/K	r	$\sigma/\mathrm{hPa\,d^{-1}}$	r	σ/K	r	σ/K	r	$\sigma/\mathrm{hPa\,d^{-1}}$
NP	0.16	1.5	**0.64**	**2.6**	0.74	10.3	**-0.83**	0.6	0.76	**0.7**	-0.08	5.4
NA	0.26	2.4	**0.49**	**3.5**	0.88	5.3	-0.53	0.5	**0.75**	**0.8**	-0.23	3.2
SI	0.52	1.8	**0.79**	**3.3**	-0.82	8.1	**-0.84**	0.7	0.72	0.7	0.00	5.4
SP	**-0.97**	**2.0**	-0.73	1.0	0.04	4.4	-0.48	0.4	**0.85**	**0.9**	0.00	6.9
SA	**-0.94**	**2.0**	-0.52	1.1	0.59	3.7	**-0.66**	0.4	0.64	**0.5**	0.26	4.9

Table 1. Correlation (r) with EIS and standard deviation (σ), respectively, for the quantities $\theta_{1000,\mathrm{c}}$, $\theta_{700,\mathrm{c}}$, and $\omega_{700,\mathrm{H}}$ over the seasonal cycle and the interannual variability. The level with the higher correlation is denoted by bold font.

This analysis demonstrates that variations in EIS are complex and regionally dependent. It also hints at why previous studies have not reported a strong relationship between the subtropical highs and cloudiness, as might be expected if, for instance, cloudiness was primarily controlled by either variations in the temperatures at the surface, possibly driven by surface winds and ocean upwelling, or aloft, possibly driven by atmospheric subsidence. Using $\omega_{700,\mathrm{H}}$ as a factor of highs does not clearly indicate whether the variability of θ_{700} is larger or smaller than that of θ_{1000}. For the seasonal cycle, the three regions with the largest variability of the high (measured by the standard variation of $\omega_{700,\mathrm{H}}$ in Table 1) are also the regions where θ_{700} varies more than θ_{1000}. However, this relationship does not necessarily indicate a causal link between subsidence rate in the high and θ_{700}, because it does not hold on interannual timescales. Moreover, the correlation between $\omega_{700,\mathrm{H}}$ and EIS nearly vanishes, further suggesting that variations in atmospheric subsidence over H-areas are not the cause of changes in EIS.

To explore whether such relationships might exist, but are hidden by co-variability in other factors, we regress EIS against Q_{c}, the adiabatic warming in the cloud region, as well as two fields that could be indicative of the influence of the subtropical high on surface mechanisms, one being the $\mathrm{LHF_c}$, which we expect to co-vary with the surface wind speed, $\|V\|$, the other being ocean upwelling, w_{E}. Figure 3 shows that some weak relationships emerge, as expected. Greater adiabatic warming, stronger winds (as measured by surface-latent heat fluxes) and more ocean upwelling all are positively correlated with increases

in EIS. Because the relationships are generally stronger over the seasonal cycle as compared to the interannual record, it raises the question as to whether they are causal.

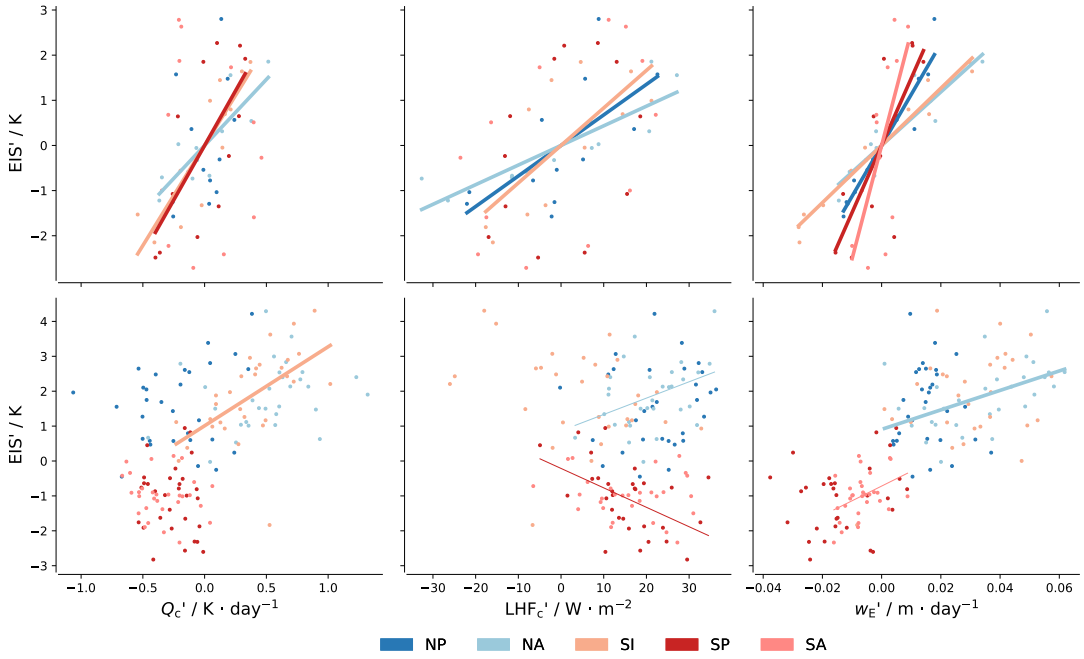

Figure 3. Scatter plots of Q and EIS (left), LHF and EIS (middle), and w_{E} and EIS (right). The primes indicate deviations from the mean of the respective regions on the corresponding timescales. Each color represents a region. The top branch is for the seasonal cycle, and the bottom branch is for the interannual time series. Regression lines are presented for p-values ≤ 0.05, and thickened when $r^2 \geq 0.25$.

3.2 Control by atmospheric subsidence

Before exploring to what extent variations in the high-pressure regions can explain variations in θ_{700} we first examine the more basic question as to whether the adiabatic warming, which in stationarity balances the diabatic cooling Q, co-varies with ω_{700} in the Sc areas. Fig. 4 demonstrates that there is a clear relationship between Q_{c} at 700 hPa and $\omega_{700,\mathrm{c}}$ in the climatological mean (Fig. 4). A strong and consistent relationship also emerges across the seasonal cycle and on interannual timescales (Fig. 5). Hence $\omega_{700,\mathrm{H}}$ is a good proxy for the adiabatic warming in the cloud areas.

Knowledge of the adiabatic warming is, however, not sufficient to determine θ_{700}. This is shown in Fig. 6, which shows no consistent relationship between Q_{c} and $\theta_{700,\mathrm{c}}$ across the seasonal cycle for the different regions, and no relationship between Q_{c} and $\theta_{700,\mathrm{c}}$ whatsoever on interannual timescales. This indicates that $\omega_{700,\mathrm{c}}$ is not the dominant factor for changes in θ_{700}, and falsifies the hypothesis that variations in $\theta_{700,\mathrm{c}}$ can be explained by a monsoon-desert mechanism, at least one mediated by the adiabatic warming.

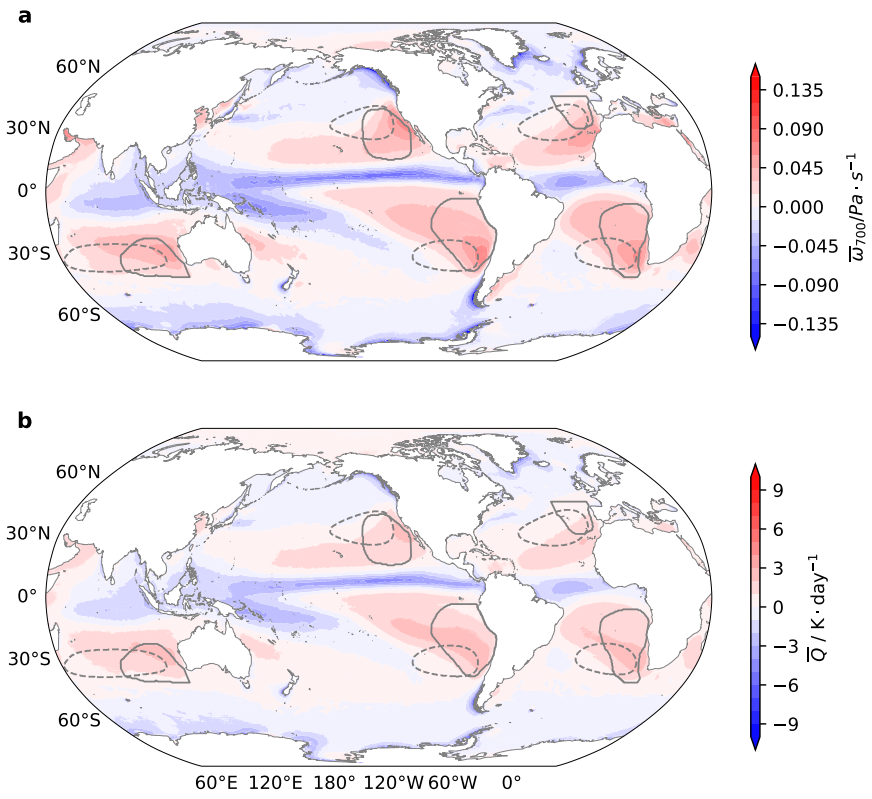

Figure 4. Map of 1985–2014 climatological mean ω_{700} (top) and Q (bottom). Subtropical high areas are shown by dashed lines and cloud-regions are outlined by solid lines.

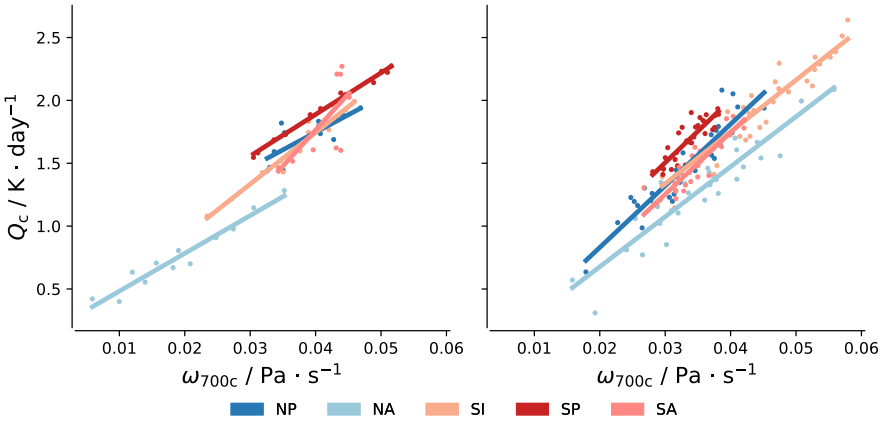

Figure 5. Scatter plots of ω_{700} and Q. Subscript c denotes the mean value of the variable in the c-area. Each color represents a region. The left subplot is for the seasonal cycle, and the right subplot is for the interannual time series. Regression lines are presented for p-values $\leq$ 0.05, and thickened when $r^2 \geq 0.25$.

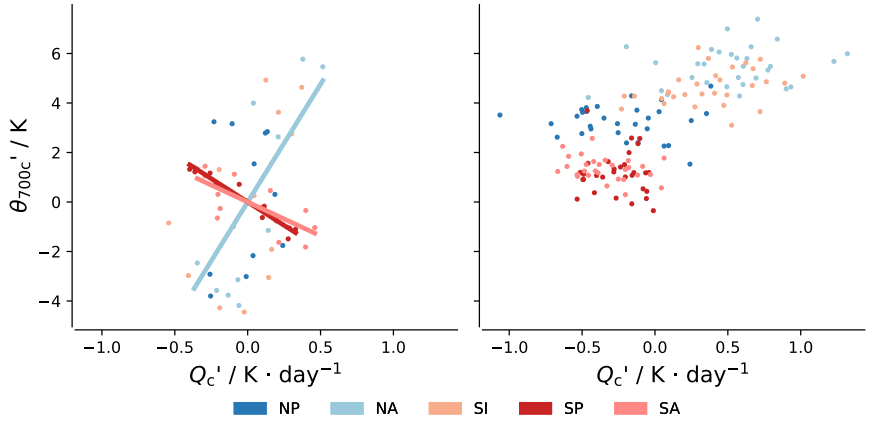

Figure 6. Scatter plots of Q and θ_{700}. The primes indicate deviations from the mean of the respective regions on the corresponding timescales. Subscript c denotes the mean value of the variable in the c-area. Each color represents a region. The left subplot is for the seasonal cycle, and the right subplot is for the interannual time series. Regression lines are presented for p-values ≤ 0.05, and thickened when $r^2 \geq 0.25$.

3.3 Control by wind-driven cooling

In addition to subsidence rates, the steepness of subtropical highs is also proposed to influence EIS. As subtropical highs are typically located on the western flanks of Sc, the steepness of highs may affect the zonal geopotential gradient in c-areas, and thereby impact near-surface winds there. According to Sverdrup balance, the equatorward near-surface wind, which in geostrophic balance is determined by the zonal geopotential gradient ($\frac{\mathrm{d}\Phi}{\mathrm{d}x}$), is associated with a wind-stress gradient that results in ocean Ekman pumping (Anderson and Gill, 1975). In addition, the changed near-surface wind can also affect cold advection of waters from high-latitudes, and impact surface evaporative cooling as measured by the surface latent heat flux (LHF).

Figure 7 shows patterns for mean $\frac{\mathrm{d}\Phi}{\mathrm{d}x}$, Ekman pumping velocity (w_{E}), and LHF. Unlike Q and ω_{700}, pattern correlations are difficult to discern. Ocean upwelling areas are restricted to the coastal regions where the wind-stress curl is large, and the maximum LHF is located on the west and equatorward side of the maximum $\frac{\mathrm{d}\Phi}{\mathrm{d}x}$ where temperatures are warmer and strong trade-winds prevail. A more quantitative evaluation of the relationship between $\frac{\mathrm{d}\Phi}{\mathrm{d}x}$ and either w_{E} or LHF (not shown), does not show strong and consistent relationships across regions or timescales. This leads us to conclude that variations in near-surface geopotential gradients are not the primary driver of changes in θ_{1000} (Fig. 8) and hence variations in EIS.

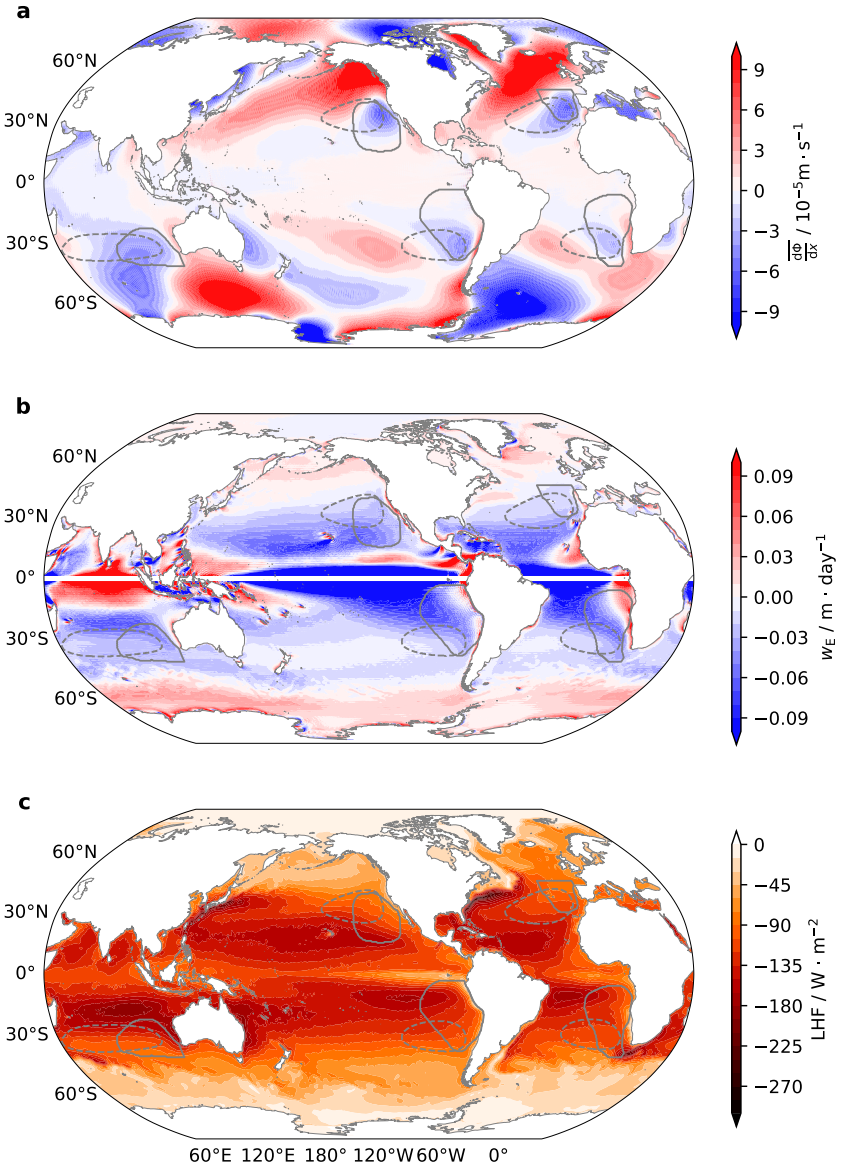

Figure 7. Map of 1985–2014 climatological mean a. $\frac{\mathrm{d}\Phi}{\mathrm{d}x}$, b. w_{E} (masked within 1°N–1°S), c. LHF.

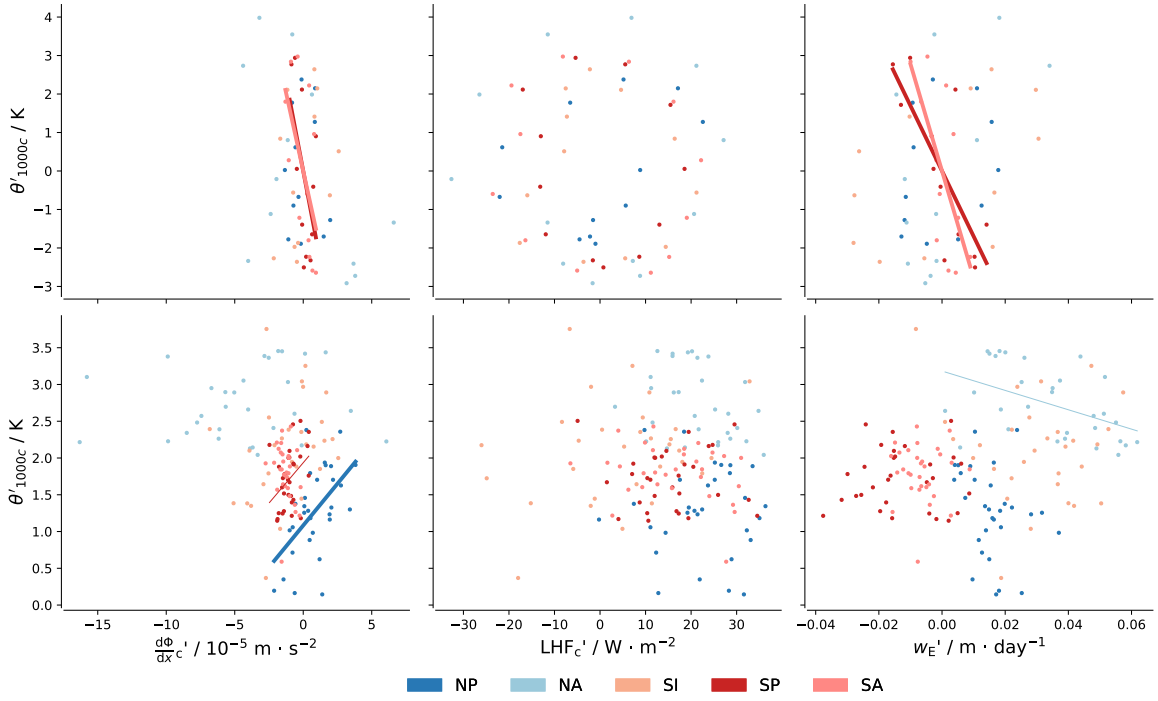

Figure 8. Scatter plots of $\frac{\mathrm{d}\Phi}{\mathrm{d}x}$ and θ_{1000} (left), LHF and θ_{1000} (middle), and w_{E} and θ_{1000} (right). Subscript c denotes the mean value of the variable in the c-area, while w_{E} is averaged over the continuous ocean upwelling area near the coast. The primes indicate deviations from the mean of the respective regions on the corresponding timescales. Each color represents a region. The top branch is for the seasonal cycle, and the bottom branch is for the interannual time series. Regression lines are presented for p-values ≤ 0.05, and thickened when $r^2 \geq 0.25$.

3.4 The disconnection between changes in H- and c- areas

Until this point we have considered proxies within c-areas for the variation of H-areas that generally lie westward of c-areas. Figure 9 shows that subsidence in c-areas is not necessarily a good proxy for subsidence in H-areas,, as no rule for the relationships between H- and c- areas emerges (left column). Correlations, when they exist can differ in sign across regions and for the same region across timescales. Even though the regression coefficients between the two areas show some similarity in NA across timescales, the correlations in the interannual time series are weak. In addition, subsidence can vary at different rates from SLP in H-areas (right column). Figure 10 also shows that geopotential gradient in c-areas does not consistently correlate with SLP in H-areas. Therefore, the properties of c-areas that may affect EIS do not simply follow the strength of subtropical highs, which further reduces the probability of predicting Sc by subtropical highs.

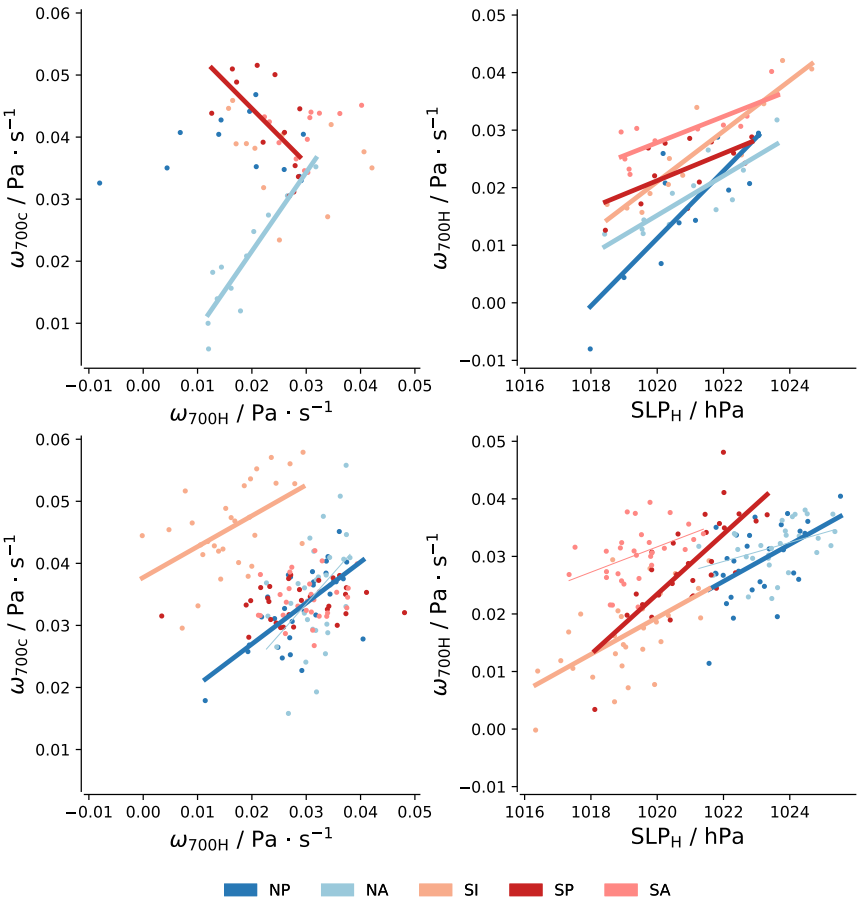

Figure 9. Scatter plots of ω_{700} between H- and c- areas (left), and ω_{700} and SLP in H-areas (right). Each color represents a region. The top branch is for the seasonal cycle, and the bottom branch is for the interannual time series. Regression lines are presented for p-values ≤ 0.05, and thickened when $r^2 \geq 0.25$.

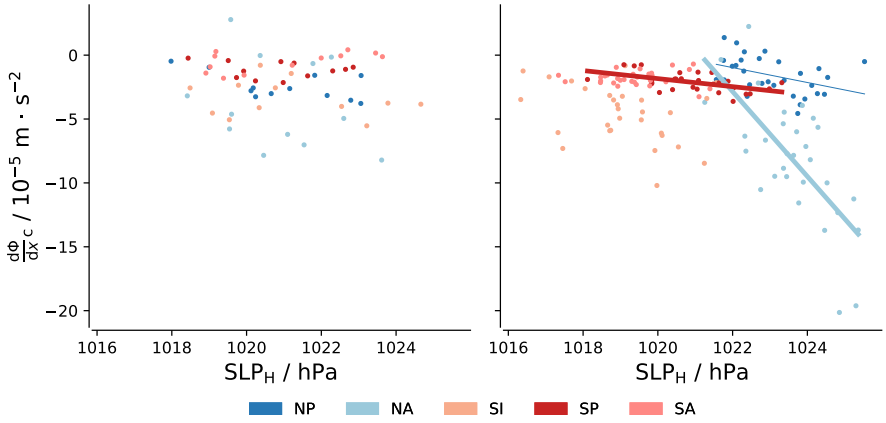

Figure 10. Scatter plots of $\frac{\mathrm{d}\Phi}{\mathrm{d}x}$ in c-areas and SLP in H-areas on the seasonal (left) and interannual (right) timescales. Each color represents a region. Regression lines are presented for p-values ≤ 0.05, and thickened when $r^2 \geq 0.25$.

4 Conclusions

This paper tests two hypothesized mechanisms by which subtropical highs may affect Sc. Both hypotheses are rejected.

First we define the marine high-pressure areas and the Sc areas by a surface isobar in the case of the former and a satellite derived cloud fraction in the latter. This identifies five regions, in each of which the high-pressure area intersects the Sc area, with the latter generally locates on the eastward flanks of the former. Next we demonstrate that Sc is well predicted by both the lower-tropospheric stability (LTS) and the Estimated Inversion Strength (EIS). A more recent proposal for a cloud controlling factor, the Estimated Cloud Top Entrainment Index, is more complex as it includes humidity variations and does not perform better than the EIS, as its additional skill arises from predictions outside of the main cloud areas we consider. Furthermore, in the areas we consider, and for any particular region, most of the variability in EIS can be explained by LTS alone.

Given these findings we hypothesize that EIS (or LTS) can be increased through an increase in adiabatic warming, Q, which maintains a higher potential temperature at $700\,\mathrm{hPa}$. An enhanced subsidence in subtropical highs can lead to this increase in adiabatic warming. However, the variation of Q is not the dominant factor influencing changes in temperature above Sc (θ_{700}), as the correlation of θ_{700} and adiabatic warming can even be negative in some regions. This agrees with (Caldwell and Bretherton, 2009), which shows that the effects of the thermodynamic process are not warming the free troposphere directly; instead, it works more on enhancing the subsidence itself, which all things considered would maintain a shallower cloud layer.

We further hypothesize that the steepness of the subtropical highs could modulate Sc amounts through their effect on the surface momentum balance, and hence surface temperature, to which θ_{1000} is strongly related. A high with larger geopotential gradient in the Sc area is posited to increase surface wind speeds, enhancing ocean upwelling (w_E) along eastern coasts, accompanied by greater surface evaporation and cooling. If this mechanism were a dominant factor in controlling θ_{1000}, we would expect strong relationships between θ_{1000} and both w_E and latent heat flux (LHF), as well as a correlation between geopotential gradient and w_E, and even with LHF. However, there is little evidence supporting these relationships.

Environmental changes associated with variations in the subtropical high-pressure regions correlate better with LTS (and EIS) than they do with the components of the LTS and EIS the variations are thought to influence. On both seasonal and interannual timescales regionally unified positive correlations between Q and EIS, as well as between ocean upwelling velocity and EIS can be identified. We interpret this as indicative of variations in high-pressure regions not being the primary cause of variations in the Q, w_E or LHF, but rather indicative of hidden mechanisms that cause these quantities to co-vary with LTS. This finding is further supported by the lack of robust relationships between the variations in Q, w_E or LHF, in the high-pressure region and the same quantity in the partially overlapping cloud regions.

Our results do not support the hypotheses that an understanding of how the subtropical highs change with climate will be informative for how Sc amount will change in regions where such clouds prevail. It is well appreciated that the temperature control of the convecting areas on the moist adiabatic lapse rate throughout the tropics can influence the near tropical LTS (Manabe et al., 1965; Stone and Carlson, 1979; Betts, 1986). However, there is also a growing appreciation of the departures from the weak-temperature gradients that this mechanism relies on, which will continue to motivate efforts to identify dynamic

factors influencing the LTS across the near tropics (Sobel and Bretherton, 2000; Sobel et al., 2001; Singh and O'Gorman, 2013; Bao and Stevens, 2021).

Data availability. The data sets used in this work can be obtained from the ERA5 and ATSR-AATSR online repositories at https://www.ecmwf.int/en/forecasts/datasets/reanalysis-datasets/era5 and http://catalogue.ceda.ac.uk/uuid/1ea3b2e391e4441daa57100a02b98691.

Author contributions. HD did the data process and analyses, and wrote the original draft of this paper and edited it later. BS proposed the idea, restructured the paper, and wrote the analyses. HS reviewed and edited this paper, contributed to discussions, and helped guide the analyses.

Competing interests. The authors declare that no competing interests are present.

Acknowledgements. The German Climate Computation Centre (DKRZ) provided the reanalysis data and supercomputer used in this study. The authors appreciate their support for the data pool and server. The authors also appreciate Hans Segura, Tiffany Shaw, Nedjeljka Zagar, Ian Dragaud, and Marco Giorgetta, who shared their thoughts that influenced this paper.

References

Anderson, D. and Gill, A.: Spin-up of a stratified ocean, with applications to upwelling, Deep Sea Research and Oceanographic Abstracts, 22(9), 583–596, https://doi.org/10.1016/0011-7471(75)90046-7, 1975.

Bao, J. and Stevens, B.: The elements of the thermodynamic structure of the tropical atmosphere, Journal of the Meteorological Society of Japan, Ser. II, 99(6), 1483–1499, https://doi.org/10.2151/jmsj.2021-072, 2021.

Betts, A.: A new convective adjustment scheme. Part I: Observational and theoretical basis, Quarterly Journal of the Royal Meteorological Society, 112(473), 677–691, https://doi.org/10.1002/qj.49711247307, 1986.

Blake, D.: Temperature inversions at San Diego, as deduced from aerographical observations by airplane, Monthly Weather Review, 56(6), 221–224, https://doi.org/10.1175/1520-0493(1928)56<221:TIASDA>2.0.CO;2, 1928.

Caldwell, P. and Bretherton, C.: Response of a subtropical stratocumulus-capped mixed layer to climate and aerosol changes, Journal of climate, 22(1), 20–38, https://doi.org/10.1175/2008JCLI1967.1, 2009.

Ciesielski, P., Schubert, W., and Johnson, R.: Diurnal variability of the marine boundary layer during ASTEX, Journal of the Atmospheric Sciences, 58(16), 2355–2376, https://doi.org/10.1175/1520-0469(2001)058<2355:DVOTMB>2.0.CO;2, 2001.

Cutler, L., Brunke, M., and Zeng, X.: Re-evaluation of low cloud amount relationships with lower-tropospheric stability and estimated inversion strength, Geophysical Research Letters, 136(11), e2022GL098 137, https://doi.org/10.1029/2022GL098137, 2022.

Duynkerke, P. and Teixeira, J.: Comparison of the ECMWF reanalysis with FIRE I observations: Diurnal variation of marine stratocumulus, Journal of climate, 14(7), 1466–1478, https://doi.org/10.1175/1520-0442(2001)014<1466:COTERW>2.0.CO;2, 2001.

Garreaud, R. and Muñoz, R.: The diurnal cycle in circulation and cloudiness over the subtropical southeast Pacific: A modeling study, Journal of climate, 17(8), 1699–1710, https://doi.org/10.1175/1520-0442(2004)017<1699:TDCICA>2.0.CO;2, 2004.

George, R. and Wood, R.: Subseasonal variability of low cloud radiative properties over the southeast Pacific Ocean, Atmospheric Chemistry and Physics, 10(8), 4047–4063, https://doi.org/10.5194/acp-10-4047-2010, 2010.

Hahn, C. and Warren, S.: A gridded climatology of clouds over land (1971-96) and ocean (1954-97) from surface observations worldwide, Oak Ridge, TN: Oak Ridge National Laboratory, Carbon Dioxide Information Analysis Center, 2007.

Hartmann, D. and Short, D.: On the use of earth radiation budget statistics for studies of clouds and climate, Journal of Atmospheric Sciences, 37(6), 1233–1250, https://doi.org/10.1175/1520-0469(1980)037<1233:OTUOER>2.0.CO;2, 1980.

Hersbach, H., Bell, B., Berrisford, P., Hirahara, S., Horányi, A., Muñoz-Sabater, J., Nicolas, J., Peubey, C., Radu, R., Schepers, D., Simmons, A., Soci, C., Abdalla, S., Abellan, X., Balsamo, G., Bechtold, P., Biavati, G., Bidlot, J., Bonavita, M., De Chiara, G., Dahlgren, P., Dee, D., Diamantakis, M., Dragani, R., Flemming, J., Forbes, R., Fuentes, M., Geer, A., Haimberger, L., Healy, S., Hogan, R., Hólm, E., Janisková, M., Keeley, S., Laloyaux, P., Lopez, P., Lupu, C., Radnoti, G., de Rosnay, P., Rozum, I., Vamborg, F., Villaume, S., and Thépaut, J.-N.: Complete ERA5 from 1940: Fifth generation of ECMWF atmospheric reanalyses of the global climate, Copernicus Climate Change Service (C3S) Data Store (CDS), https://doi.org/10.24381/cds.143582cf (Accessed on 15-JUN-2023), 2017.

Kawai, H., Koshiro, T., and Webb, M.: Interpretation of Factors Controlling Low Cloud Cover and Low Cloud Feedback Using a Unified Predictive Index, Journal of Climate, 30, 9119–9131, https://doi.org/10.1175/JCLI-D-16-0825.1, 2017.

Klein, S.: Synoptic variability of low-cloud properties and meteorological parameters in the subtropical trade wind boundary layer, Journal of Climate, 10(8), 2018–2039, https://doi.org/10.1175/1520-0442(1997)010<2018:SVOLCP>2.0.CO;2, 1997.

Klein, S. and Hartmann, D.: The seasonal cycle of low stratiform clouds, Journal of Climate, 6(8), 1587–1606, https://doi.org/10.1175/1520-0442(1993)006<1587:TSCOLS>2.0.CO;2, 1993.

Klein, S., Hartmann, D., and Norris, J.: On the relationships among low-cloud structure, sea surface temperature, and atmospheric circulation in the summertime northeast Pacific, Journal of climate, 8(5), 1140–1155, https://doi.org/10.1175/1520-0442(1995)008<1140:OTRALC>2.0.CO;2, 1995.

Large, W. G. and Pond, S.: Open ocean momentum flux measurements in moderate to strong winds, Journal of physical oceanography, 11(3), 324–336, https://doi.org/10.1175/1520-0485(1981)011<0324:OOMFMI>2.0.CO;2, 1981.

Lawrence, M. G.: The relationship between relative humidity and the dewpoint temperature in moist air: A simple conversion and applications, Bulletin of the American Meteorological Society, 86(2), 225–234, https://doi.org/10.1175/BAMS-86-2-225, 2005.

Manabe, S., Smagorinsky, J., and Strickler, R.: Simulated climatology of a general circulation model with a hydrologic cycle, Monthly Weather Review, 93(12), 769–798, https://doi.org/10.1175/1520-0493(1965)093<0769:SCOAGC>2.3.CO;2, 1965.

McCoy, D., Eastman, R., Hartmann, D., and Wood, R.: The change in low cloud cover in a warmed climate inferred from AIRS, MODIS, and ERA-Interim, Journal of climate, 30(10), 3609–3620, https://doi.org/10.1175/JCLI-D-15-0734.1, 2017.

Park, S. and Shin, J.: Heuristic estimation of low-level cloud fraction over the globe based on a decoupling parameterization, Atmospheric Chemistry and Physics, 19(8), 5635–5660, https://doi.org/10.5194/acp-19-5635-2019, 2019.

Poulsen, C., McGarragh, G., Thomas, G., Christensen, M., Povey, A., Grainger, D., Proud, S., and Hollmann, R.: ESA Cloud Climate Change Initiative (Cloud_cci): ATSR2-AASTR monthly gridded cloud properties, version 2.0, https://catalogue.ceda.ac.uk/uuid/1ea3b2e391e4441daa57100a02b98691, accessed 16 Feburary 2023, 2017.

Qu, X., Hall, A., Klein, S., and DeAngelis, A.: Positive tropical marine low-cloud cover feedback inferred from cloud-controlling factors, Geophysical Research Letters, 42(18), 7767–7775, https://doi.org/10.1002/2015GL065627, 2015.

Randall, D. and Suarez, M.: On the dynamics of stratocumulus formation and dissipation, Journal of Atmospheric Sciences, 41(20), 3052–3057, https://doi.org/10.1175/1520-0469(1984)041<3052:OTDOSF>2.0.CO;2, 1984.

Richter, I. and Mechoso, C.: Orographic influences on the annual cycle of Namibian stratocumulus clouds, Geophysical Research Letters, 31(24), L24 108, https://doi.org/10.1029/2004GL020814, 2004.

Richter, I. and Mechoso, C.: Orographic influences on subtropical stratocumulus, Journal of the Atmospheric Sciences, 63(10), 2585–2601, https://doi.org/10.1175/JAS3756.1, 2006.

Rodwell, M. and Hoskins, B.: Monsoons and the dynamics of deserts, Quarterly Journal of the Royal Meteorological Society, 122(534), 1385–1404, https://doi.org/10.1002/qj.49712253408, 1996.

Singh, M. and O'Gorman, P.: Influence of entrainment on the thermal stratification in simulations of radiative-convective equilibrium, Geophysical Research Letters, 40(16)), 4398–4403, https://doi.org/10.1002/grl.50796, 2013.

Slingo, A.: Sensitivity of the Earth's radiation budget to changes in low clouds, Nature, 343(6253), 49–51, https://doi.org/10.1038/343049a0, 1990.

Sobel, A. and Bretherton, C.: Modeling tropical precipitation in a single column, Journal of climate, 13(24), 4378–4392, https://doi.org/10.1175/1520-0442(2000)013<4378:MTPIAS>2.0.CO;2, 2000.

Sobel, A., Nilsson, J., and Polvani, L.: The weak temperature gradient approximation and balanced tropical moisture waves, Journal of the Atmospheric Sciences, 58(23), 3650–3665, https://doi.org/10.1175/1520-0469(2001)058<3650:TWTGAA>2.0.CO;2, 2001.

Stevens, B. and Brenguier, J.: Cloud controlling factors: low clouds, in: Clouds in the perturbed climate system: their relationship to energy balance, atmospheric dynamics, and precipitation, edited by: Heintzenberg, J. and Charlson, R. J., MIT Press, p. 173–196, https://doi.org/10.7551/mitpress/8300.003.0010, 2009.

Stone, P. and Carlson, J.: Atmospheric lapse rate regimes and their parameterization, Journal of the Atmospheric Sciences, 36(3), 415–423, https://doi.org/10.1175/1520-0469(1979)036<0415:ALRRAT>2.0.CO;2, 1979.

Toniazzo, T., Abel, S., Wood, R., Mechoso, C., Allen, G., and Shaffrey, L.: Large-scale and synoptic meteorology in the south-east Pacific during the observations campaign VOCALS-REx in austral Spring 2008, Atmospheric Chemistry and Physics, 11(10), 4977–5009, https://doi.org/10.5194/acp-11-4977-2011, 2011.

Warren, S., Hahn, C., London, J., Chervin, R., and Jenne, R.: Global Distribution of Total Cloud Cover and Cloud Type Amounts Over Land (No. NCAR/TN-273+STR), University Corporation for Atmospheric Research, 29, + 200 maps, https://doi.org/10.5065/D6GH9FXB, 1986.

Warren, S., Hahn, C., London, J., Chervin, R., and Jenne, R.: Global Distribution of Total Cloud Cover and Cloud Type Amounts Over the Ocean (No. NCAR/TN-317+STR), University Corporation for Atmospheric Research, 42, + 170 maps, https://doi.org/10.5065/D6QC01D1, 1988.

Weaver, C. and Pearson Jr, R.: Entrainment instability and vertical motion as causes of stratocumulus breakup, Quarterly Journal of the Royal Meteorological Society, 116(496), 1359–1388, https://doi.org/10.1002/qj.49711649606, 1990.

Wood, R.: Stratocumulus Clouds, Atmos. Chem. Phys., 140, 2373–2423, https://doi.org/10.1175/MWR-D-11-00121.1, 2012.

Wood, R. and Bretherton, C.: On the relationship between stratiform low cloud cover and lower-tropospheric stability, Journal of Climate, 19, 6425–6432, https://doi.org/10.1175/JCLI3988.1, 2006.

Zhou, C., Zelinka, M., Dessler, A., and Klein, S.: The relationship between interannual and long-term cloud feedbacks, Geophysical Research Letters, 42(23), 10–463, https://doi.org/10.1002/2015GL066698, 2015.